Cluster analysis in remote sensing spectral imagery through graph representation and advanced SOM visualization

Kadim Taşdemir[1] and Erzsébet Merényi[1] *

Rice University, Electrical and Computer Engineering
6100 Main Street, Houston, TX, 77005 - USA

Abstract. The Self-Organizing Map (SOM), a powerful method for clustering and knowledge discovery, has been used effectively for remote sensing spectral images which often have high-dimensional feature vectors (spectra) and many meaningful clusters with varying statistics. However, a learned SOM needs postprocessing to identify the clusters, which is typically done interactively from various visualizations. What aspects of the SOM's knowledge are presented by a visualization has great importance for cluster capture. We present our recent scheme, CONNvis, which achieves detailed delineation of cluster boundaries by rendering data topology on the SOM lattice. We show discovery through CONNvis clustering in a remote sensing spectral image from the Mars Exploration Rover Spirit.

1 Introduction

Self-Organizing Maps (SOMs) are widely and successfully used neural paradigms for clustering and data mining. They perform an iterative learning process which has two advantageous properties: an adaptive vector quantization that results in optimal placement of the prototypes in the data space; and ordering of those prototypes on a rigid low-dimensional lattice according to their similarities. Due to these properties, SOMs facilitate informative visualization of the structure of a higher-dimensional data space in lower (usually two) dimensions, which in turn aids interactive capture of the cluster boundaries.

Many visualization schemes have been proposed to represent distance based (dis)similarities of prototypes or the size of the receptive fields of neural units in various ways such as by screen intensity levels, or by the sizes or shapes of the SOM grid cells. The most commonly used methods include the U-matrix [1] and its variants, which represent the (Euclidean) distance of the prototypes that are neighbors in the SOM lattice. These are useful when relatively large SOM grid

* This work was partially supported by grant NNG05GA94G from the Applied Information Systems Research Program, NASA, Science Mission Directorate. We thank Dr. William Farrand from the Space Science Institute, Boulder, CO, USA for his valuable contributions to the analysis of the Martian scene discussed here. Figures are in color, request color copy by email: tasdemir@rice.edu, erzsebet@rice.edu

accomodates small data sets with a low number of clusters (e.g., [2], [3]) but, because of averaging of prototype distances over neighbours or thresholding, they tend to miss finer structure in complicated data [4]. Alternatively, the distances between neighboring prototypes are shown through the adaptation of the size or the shape of the grid cells [5, 6]. Another approach for visual inspection is a modified SOM algorithm which updates the grid positions of prototypes based on their similarities instead of having a rigid grid (Adaptive Coordinates [7], Double SOM [8], visualization induced SOM (ViSOM) [9]). However, these either have hard-to-set parameters or are only applicable to small data sets because they require relatively large number of prototypes. Automated color assignments are also used for exploration of the coarse cluster structure [10–13]. It is popular to analyze individual component planes of the SOM to discover information specific to the corresponding component [12, 14]. We point the reader to [14] and [15] for more review.

A recent graph-based SOM visualization, CONNvis, proposed by these authors [16], represents the data topology by a weighted version of the Delaunay graph and drapes this graph over the SOM. In this paper, we show how CONNvis helps detailed interactive cluster capture and knowledge discovery from remote sensing spectral imagery, through an example of a Martian scene. Section 2 briefly explains CONNvis and clustering. Section 3 discusses the application to Martian geology. Section 4 concludes and provides future directions.

2 CONNvis: A graph based SOM visualization

CONNvis is a rendering of data topology – represented by a "connectivity matrix" CONN – on the SOM lattice [15]. Below we first describe CONN, then how it is used as a SOM visualization to assist interactive clustering.

2.1 Connectivity matrix (CONN)

The connectivity matrix [15], CONN, is a weighted Delaunay triangulation, where the weight of an edge connecting two prototypes is the number of data vectors for which these prototypes are the best matching unit (BMU) and the second BMU. Formally, each element of CONN, $CONN(i, j)$, *the connectivity strength* between prototypes i and j is defined as

$$CONN(i, j) = |RF_{ij}| + |RF_{ji}| \tag{1}$$

where RF_{ij} is that section of the receptive field (Voronoi polyhedron) of the prototype i where j is the second BMU, and $|RF_{ij}|$ is the number of data vectors in RF_{ij}. CONN thus shows how the data is distributed within the receptive fields with respect to neighbor prototypes. This produces a finer density distribution than other existing density representations which show the distribution on the receptive field level. CONN also indicates the neighborhood relations of the prototypes with respect to the data manifold because a binarized CONN is equivalent to the *induced* Delaunay graph, which is the intersection of the

Delaunay triangulation with the data manifold [17]. This results in making the separations within the data set visible.

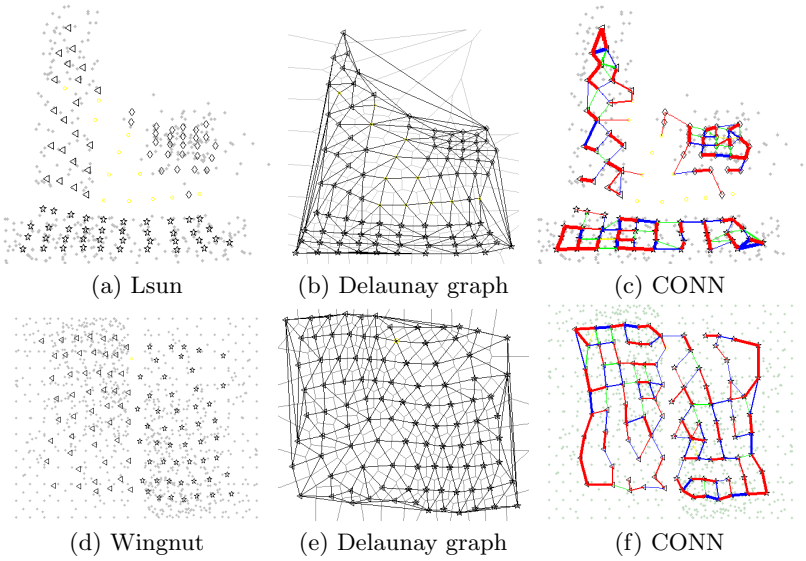

(a) Lsun (b) Delaunay graph (c) CONN

(d) Wingnut (e) Delaunay graph (f) CONN

Fig. 1. Illustration of how the connectivity matrix CONN shows neighborhood relations in the data space, with two simple 2-d data sets from [18]. A 10×10 SOM is used to obtain prototypes. Top: (a) Lsun (3 clusters) and its prototypes with true labels in data space. (b) Delaunay triangulation of the Lsun prototypes. Empty prototypes do not have symbols. (c) CONN of Lsun prototypes. Bottom: (d) Wingnut (2 clusters with inhomogeneous density distribution) (e) Delaunay triangulation of the Wingnut prototypes (f) CONN of Wingnut prototypes. The clusters of Lsun and Wingnut can be seen through the CONN.

Fig. 1 shows examples of CONN for two simple 2-d data sets constructed by [18]. The first one is called "Lsun" which has three well-separated clusters (two rectangular and one spherical). The second one, "Wingnut", has two rectangular clusters with inhomogeneous density distribution within clusters and similar intra-cluster and inter-cluster distances. For both cases, the cluster structure can be seen through CONN regardless of the variations in cluster characteristics. CONN can be visualized in the data space for low-d (1-d to 3-d) data sets. For high-d data sets, it can be rendered on the 2-d SOM lattice to represent the data topology just as informatively as in the data space, as shown in Fig. 2.

2.2 CONNvis: Rendering CONN on the SOM

CONN can be visualized on the SOM by connecting the lattice locations of the prototypes with lines of various widths and colors. The line widths are made proportional to the connectivity strengths, $CONN(i, j)$, thus show the density distribution among the connected units. The line width conveys a sense of the *global* importance of each connection by allowing comparison with all others,

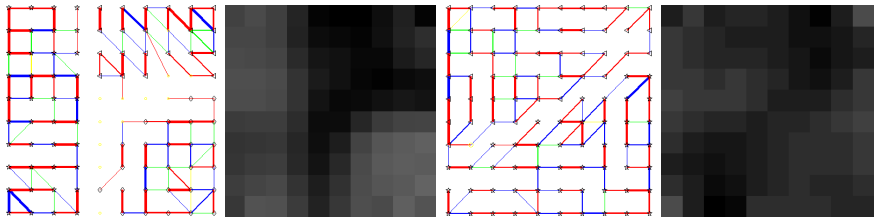

(a) CONNvis (b) U-matrix (c) CONNvis (d) U-matrix

Fig. 2. CONNvis and U-matrix visualization of the 10x10 SOM prototypes of the two datasets in Fig. 1. (a) CONNvis of the Lsun. 3 clusters are visually separated through CONNvis. (b) U-matrix of Lsun. A darker grey indicates more dissimilarity. It is hard to see the 3 clusters from this visualization. (c) CONNvis of the Wingnut. 2 clusters are made visible by strong connectivity within themselves but only one weak connection across them. (d) U-matrix of Wingnut. Due to equal distances between prototypes within and across clusters, it is hard to see the separation between two clusters.

in this visualization. Line colors are used to express a ranking of the Voronoi neighbors of a prototype i in terms of the strengths of their connectivity to i : the most-to-least connected neighbors are shown with red, blue, green, yellow, and dark to light grey colors, in this order. Since this ranking does not depend on the size of the receptive field of i, but only on the relative contribution of each neighbor, the line color indicates the *local* importance of a connection. It also defines a similarity measure among the neighbors.

Fig. 2 shows examples of CONN rendered on the 10×10 SOM of the two small data sets in Fig. 1. The separations (clusters) in the data can be clearly seen through the CONNvis in Figures 2.a and 2.c. For the same data sets, the U-matrix does not resolve sufficient detail for visual extraction of the clusters in Lsun and Wingnut (Figures 2.b and 2.d.). A larger SOM (100×100) can discover these clusters through a U-matrix as shown in [3], at significantly larger computational cost. Explanatory examples of CONNvis for a more complicated 2-d data set are given in [15].

In CONNvis, using a different line width for each connectivity strength becomes infeasible, due to limitations by screen resolution and the discrimination capability of the human eye, when the number of data samples is much larger than the number of prototypes and consequently connectivity strengths span a large range of values.. To help this, a 4-level binning scheme is applied for line widths as follows:

$$width(i,j) = \begin{cases} 1 & \mu_3 > CONN(i,j) \geq \{\mu_4, 0\} \\ 2 & \mu_2 > CONN(i,j) \geq \mu_3 \\ 3 & \mu_1 > CONN(i,j) \geq \mu_2 \\ 4 & CONN(i,j) \geq \mu_1 \end{cases} \quad (2)$$

where $width(i,j)$ is the width of the line between prototypes i and j, μ_n is the mean strength of the n^{th} ranking connections. This choice provides an automated selection of thresholds based on internal data characteristics and also employs the limited number of bins effectively, because each bin reflects the global importance of one rank. The resolution of this binning not only distinguishes strong

connections but also reveals weak connections across densely connected SOM regions, thus those regions can be recognized as clusters as shown in Figure 3.

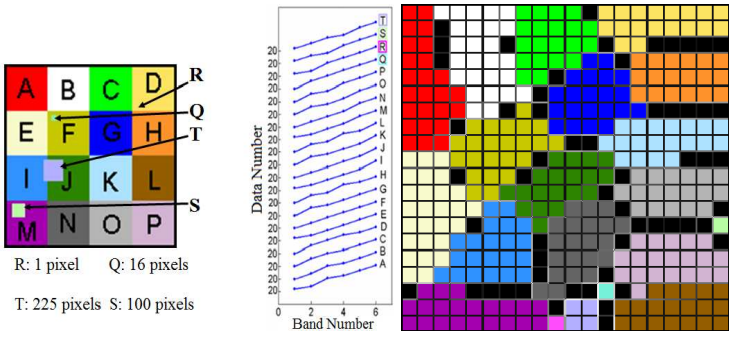

(a) 20-class, 6-d data (b) Known labels on the SOM

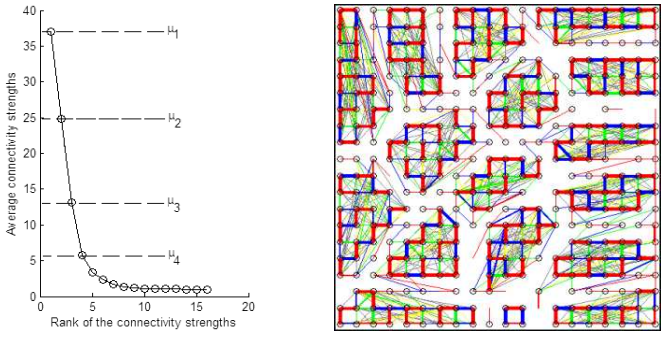

(c) The connectivity statistics (d) CONNvis

Fig. 3. (a) Left: the spatial distribution (class map) of the 20 different types of 6-d feature vectors in the 128×128 pixel image. The known types are labeled by both colors and letters. Right: the mean signatures of the 20 classes, offset for clarity. (b) Known class labels overlain on the SOM (c) Mean connectivity strengths for each rank of the connections. (d) CONNVis on the SOM. Coarse clusters (strongly connected groups of prototypes) can be detected in spite of the presence of many topology violations, *i.e.*, connections between prototypes that are not neighbors in the SOM lattice.

In Fig. 3, we analyze a 128 x 128 pixel synthetic image, where each pixel is a 6-d feature vector (the analog of a spectrum). This image has 20 classes, 4 of which are relatively small and one class has only one pixel. The signatures of these 20 classes are also similar to each other, to make clustering challenging (Fig. 3.a). A 20×20 SOM is used to obtain the quantization prototypes of this data set. The statistics of the ranked connectivity strengths in Fig. 3.c indicate that the maximum number of connections for a prototype is 16. The average connectivity strength is as high as 37 ($= \mu_1$) for the first ranking (red) connections and it drops sharply after the fourth ranking (yellow) connections ($\mu_4 = 6$). The CONNvis of this data, shown in Fig. 3.d, is obtained by using the 4-level binning scheme in eq. 2 with $\{\mu_1, \mu_2, \mu_3, 0\}$, given in Fig. 3.c, as the thresholds. It makes strongly connected groups of prototypes (coarse clusters) emerge.

Due to the representation of data topology on the SOM lattice, CONNvis also helps in a detailed assessment of topology preservation. For example, there are many grey connections in Fig. 3 which are between pairs of prototypes that are not immediate neighbors in the SOM lattice (*forward* topology violations). There are also prototypes neighbored in the SOM lattice but unconnected (which means they are not Voronoi neighbors in the data space), indicating *backward* topology violations. The more data vectors contribute to a given connection that expresses topology violation (thus termed *violating connection*), the more severe the violation. For a topology violating connection, low strength (thin line) usually indicates outliers or noise while a greater strength is due to data complexity or badly formed SOM. The *folding length* of the violating connection, that is the maximum norm distance between the connected neural units in the SOM lattice, describes whether the topology violation is local (short ranged) or global (long ranged). In [15] we define a connection as "global" if the placement of the corresponding Voronoi-neighbor prototype occurs outside of the "tightest possible" SOM neighborhood.

Similarly to the CONNvis in Fig. 3.d, perfect topology preservation is not necessary for cluster extraction in most cases. Weak global violations, or violations that remain within clusters may not affect the delineation of boundaries. However, accurate assessment of such conditions for a trained SOM is important. The connectivity matrix and its visualization, introduced above, is a useful tool for such analysis.

2.3 Interactive clustering from CONN visualization

Interactive clustering is done from CONNvis by pruning. First, topology violations are investigated and weak global ones are removed. Strong global violations require further analysis to see whether they are caused by data complexity or by bad SOM learning. For example, the CONNvis of Lsun and Wingnut, shown in Fig. 2, have no topology violations (as expected). The CONNvis of the 20-class data set (Fig. 3) has only weak violations. The global violations (as defined in [15]) will be those connections with $length > 2$ since a prototype has at most 16 neighbors in the data space (from Fig. 3.c), and these can fit in the tightest possible SOM neighborhood: 8 of them in the immediate square SOM neighborhood (at length=1) and the remaining 8 in the next tier of SOM neighborhood (at length=2). After removal of those global violations, strongly connected groups of prototypes (coarse clusters), can be seen, usually with some number of weak connections across them. The prototypes with these weak connections to the coarse clusters, i.e. prototypes at the cluster boundaries (such as shown by black dots in Fig. 4.a), are visually identified by the human analyst.

Crisp delineation of the coarse clusters is determined by evaluating the connections of those prototypes at the cluster boundaries. For any prototype at the cluster boundary, one of the three situations can occur: 1) it may have different number of connections to each cluster; 2) it may have one connection to each cluster with different strengths (widths); 3) it may have one connection to each

cluster with different ranking (color). For each situation, a corresponding criterion is applied to remove connections as follows and as illustrated in Fig. 4.a-b.

1. If the number of connections to the two cluster differs, remove the connections to the cluster with fewer connections
2. If the prototype has the same number of connections to each, remove the weaker set of connections.
3. If the prototype has the same number and strength of connections to each cluster, remove the lower ranking connection.

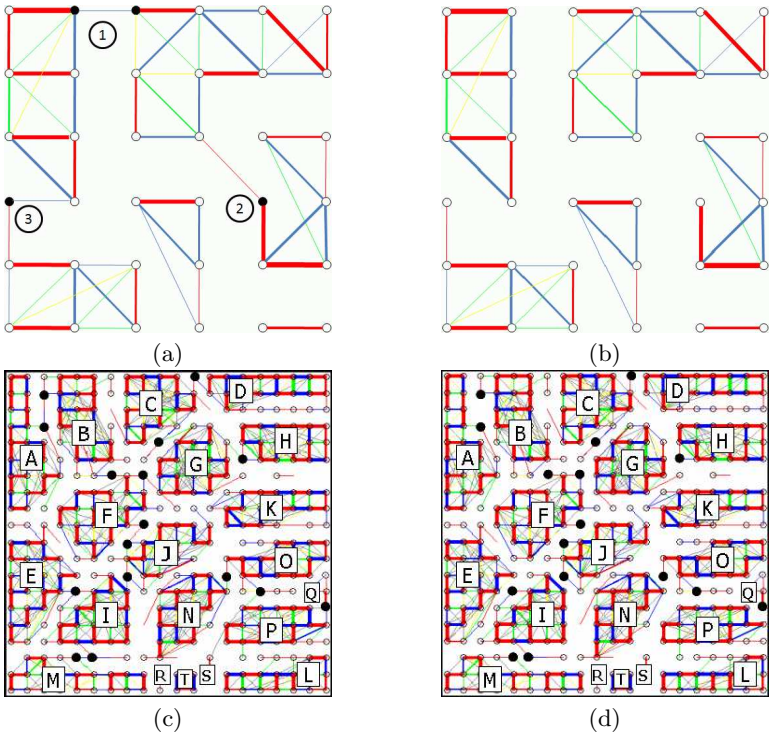

Fig. 4. Illustration of interactive clustering from CONNvis. Some groups of prototypes are outlined with the lack of connections. The prototypes at the cluster boundaries are shown by black dots. (a) The three situations at coarse cluster boundaries, for which one has to decide how to cut connections. 1: prototypes with different number of connections to each coarse cluster; 2: a prototype with the same number of connection to each cluster but with differentconnectivity strengths; 3: a prototype that has a connection to eachcluster with the same strength but different ranking. (b) Extracted clusters (separated groups of prototypes) (c) CONNvis of the 20-class data with global violations ($length > 2$) removed (d) Resulting clusters after interactive clustering. All classes, including one-pixel class R, are captured.

Figures 4.c-d illustrate the interactive clustering of the 20-class data with the above three criteria. Removal of connections across the coarse clusters results in extraction of the 20 known classes in the data, including the one pixel class R.

3 Interactive clustering of surface materials in a Mars Exploration Rover spectral image

From sol 159 of its mission to the present day, the Spirit rover has been exploring a region dubbed the Columbia Hills (in honor of the space shuttle Columbia astronauts). Rocks found in the Columbia Hills generally have clastic textures and several chemical classes have been identified [19]. These rock types have also been analyzed in terms of their visible and near infrared (VNIR) multispectral properties [20, 21] and thermal infrared emittance [22]. The scene analyzed here was collected on sol 608 of Spirit's mission near the summit of Husband Hill (named after shuttle commander Rick Husband), by the multispectral Pancam instrument. It is a 700×450 pixel 7-band image from the Pancams right "eye" (one band centered at 432 nm and six more bands with central wavelengths from 754 to 1009 nm). The image includes the rock outcrop named "Tenzing" and the rock target "Whittaker" as well as other unnamed rocks.

We use a 40×40 SOM and cluster the SOM prototypes interactively through CONNvis (Fig. 5) by visual determination of the coarse clusters and removal of the weak connections at the boundaries of these coarse clusters, as described in Section 2.2. The cluster map of the scene is shown in Fig. 6. 17 geologically meaningful clusters are extracted. Shadows and shaded regions, which do not provide geologically meaningful spectral characterization, are also shown by different grey color codes. Some clusters match well known surface units (spectral classes) identified in previous analyses [21] whereas some could be subtypes of the more representative spectral classes. Mean spectra of these 17 clusters are shown in Fig. 7 where similar spectra are placed next to each other for easy comparison of subcluster characteristics.

The far field of the scene (upper part of the image, most extensively covered by the orange class, H) is a mixture, most closely resembling the spectral signature of soil with heavy influence from rock fragments and an airfall dust component. There are also soils with presumed basaltic compositions. Some of these presumed basaltic soils (J, e) are darker-toned and coarse-grained whereas some (I, L, S) are lighter-toned and finer-grained due to much more oxidization. Among the lighter-toned soils, some (bright drift, N) are higher in albedo and are likely mobile drifts whereas some (intermediate albedo soils, L) are likely immobile. The dune near the summit of Husband Hill, which is mostly covered with bright drift (N) and intermediate albedo soil (L), is separated from the far field with a border (C, Q) that is possibly a mixture of sand grains.

The big rock (mostly covered by the orange class due to airfall dust) near the horizon is the Tenzing outcrop. Tenzing is a subtype of the Jibsheet spectral class, characterized by a shallow infrared absorption feature (centered between 900 and 934 nm) [21]. The white rocks (B) in the scene are Jibsheet type rocks whereas yellowish (D, E) rocks are rocks with a variant of the typical Jibsheet spectral signature. The slight but consistent spectral differences (Fig. 7) of two subclusters (D and E) of Tenzing may reflect different textural properties (rougher/smoother textures) of some rocks near the summit of Husband Hill (an observation by the MER team, for example, [23]). Fig. 7.b shows the slight

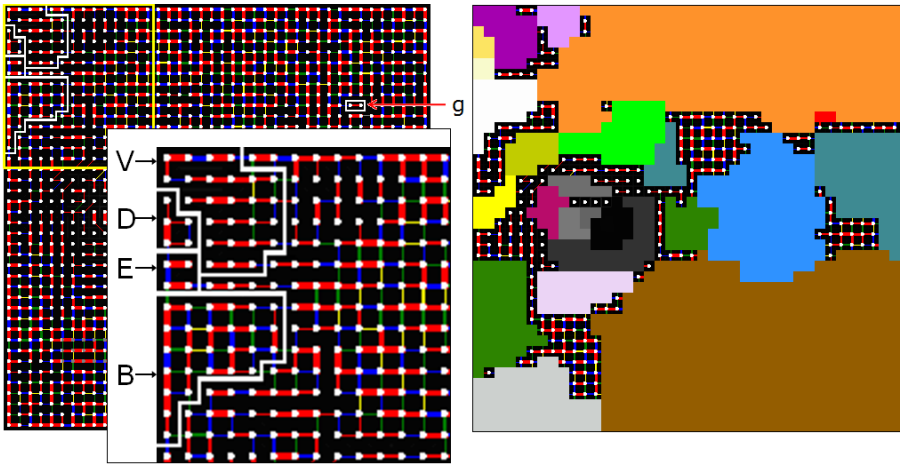

Fig. 5. Left: CONNvis of the 40×40 SOM of the Husband Hill image. The boundaries of some clusters are outlined to illustrate the results of interactive cluster extraction from CONNvis. An enlarged view of the upper left area in the yellow rectangle is shown in the inset for a clearer view. Right: Extracted clusters, color coded according to the color wedge in Fig. 6, overlain on the CONNvis. The clusters overlain on the Husband Hill image is shown in Fig. 6.

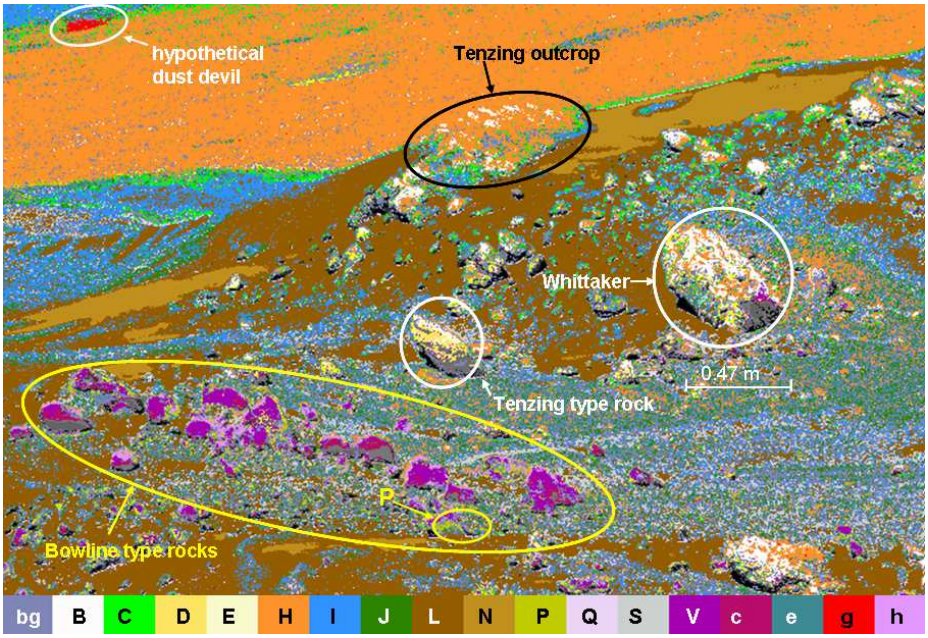

Fig. 6. Cluster map of the scene near the summit of Husband Hill (MER Pancam image taken on Sol 608) with clusters extracted from CONN visualization in Fig 5. 17 geologically meaningful clusters are color coded according to color wedge. These correspond to or refine previously identified spectral classes as explained in the text. Shaded regions are shown in various grey color codes (not included in the color wedge).

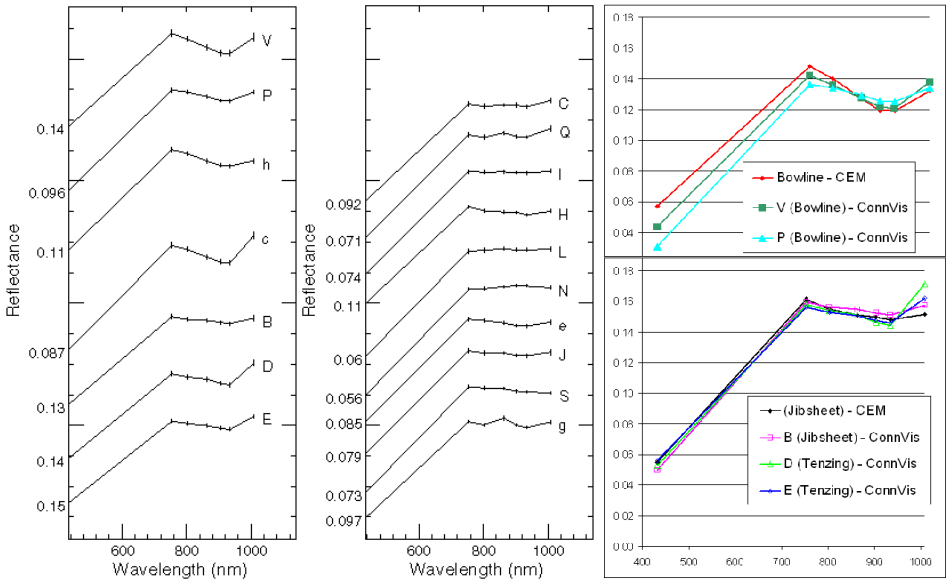

Fig. 7. Left and Center: Mean spectra of the 17 clusters in Fig. 6. The spectra of the subclusters grouped by their major types: Bowline (V, P, h), Jibsheet and Tenzing (B, D, E), soil and soil mixtures (I, H, L, N, e, J, S) and hypothetical dust devil (g). The subclusters have slight but consistent differences whereas different major types have greater spectral dissimilarities. Right: Comparison of subclusters to the corresponding superclasses in [21]. Top: Bowline subclusters. Bottom: Jibsheet and Tenzing.

differences among the spectra of subclusters B, D and E and their comparison to the Jibsheet superclass in [21]. There are also rocks in the scene which have spectra close to that of the nearby rock target Bowline. The clusters V (purple) and P (olive green) correspond to the Bowline-type rocks in the scene where P has a shallower near-infrared band compared to V and appears only in one rock. Dark purple (c) areas are partly shaded Bowline rocks whereas light pink (h) areas are a mixture of small Bowline rocks and soil.

These 17 clusters are spatially coherent and the spectral signatures of many of them have been associated with geologic meaning (either in earlier analyses, or in this analysis as geologically interpretable variations within formerly recognized classes). One cluster, g (color coded red, and shown in the white oval at the top left in Fig. 6), is a new discovery in this image. Its signature is sufficiently distinct to warrant a separate cluster, however, by analyzing the spectral relations with other classes one can arrive at a hypothesis as to the physical nature of this unit. The spectrum of g is most similar to those of sand grains (C, Q) but inherently brighter, which might be an indication of finer grains and more light scattering such as caused by fine sand stirred up in the air. The image was collected at a time of extensive dust devil activity over the far plains so one might surmise that (in spite of the poor spatial resolution that does not allow visual verification) that the unit g might be a dust devil.

In summary, through interactive CONNvis clustering, we find the geological units identified in previous analyses and segment some units into subtypes which

may be geologically meaningful. Our analysis provides a comprehensive mapping of the scene with clusters that reliably match the prototypical surface materials described by geologists. Relatively large areas, identified through our clustering as belonging to the same spectral type, have average signatures very close to the spectra of smaller type locations that were hand selected and extensively studied by geologists. By reliably showing the spatial occurrences of those materials verified from the type locations, our clusters yield trustworthy statistics for the whole scene. The reliable mapping also means potential for autonomous data analysis. This gives us confidence that CONNvis clustering can be a viable candidate for detailed information extraction and scientific discoveries.

4 Conclusions and future work

We show that CONNvis [16], a graph based visualization of data topology on the SOM lattice, successfully aids capture of accurate and fine details in remote sensing spectral imagery. This graph based visualization can also be useful for knowledge discovery from many other types of data including but not limited to genetic microarray data, genome profiles or other biological data, medical data, and financial data. Given that the parameters of CONNvis are derived automatically from the data characteristics, one might be able to apply CONN for automated cluster extraction from the SOM, with the same detail as with interactive clustering methods. This would be a significant achievement for structure discovery since current automated SOM clustering schemes produce results inferior to results from interactive procedures. This may open further possibilities for autonomous on-board science applications.

References

1. A. Ultsch, Self-organizing neural networks for visualization and classification, in: O. B. Lausen, R. Klar (Eds.), Information and Classification-Concepts, Methods and Applications, Springer Verlag, Berlin, 1993, pp. 307–313.
2. M. Kraaijveld, J. Mao, A. Jain, A nonlinear projection method based on Kohonen's topology preserving maps, IEEE Trans. on Neural Networks 6 (3) (1995) 548–559.
3. A. Ultsch, Maps for the visualization of high-dimensional data spaces, in: Proc. 4th Workshop on Self-Organizing Maps (WSOM'03), Vol. 3, 2003, pp. 225–230.
4. E. Merényi, A. Jain, Forbidden magnification? II., in: Proc. 12th European Symposium on Artificial Neural Networks (ESANN'04), Bruges, Belgium, D-Facto, April 28-30, 2004, pp. 57–62.
5. M. Cottrell, E. de Bodt, A Kohonen map representation to avoid misleading interpretations, in: Proc. 4th European Symposium on Artificial Neural Networks (ESANN'96), Bruges, Belgium, D-Facto, 1996, pp. 103–110.
6. E. Hakkinen, P. Koikkalainen, The neural data analysis environment, in: Proc. 1st Workshop on Self-Organizing Maps (WSOM'97), Espoo, Finland, June 4-6, 1997, pp. 69–74.
7. D. Merkl, A. Rauber, Alternative ways for cluster visualization in Self-Organizing Maps, in: Proc. 1st Workshop on Self-Organizing Maps (WSOM'05), Espoo, Finland, June 4-6, Helsinki University of Technology, Neural Networks Research Centre, Espoo, Finland, 1997, pp. 106–111.

8. M.-C. Su, H.-T. Chang, A new model of self-organizing neural networks and its applications, IEEE Transactions on Neural Networks 12 (1) (2001) 153–158.
9. H. Yin, ViSOM- a novel method for multivariate data projection and structure visualization, IEEE Transactions on Neural Networks 13 (1) (2002) 237–243.
10. T. Villmann, E. Merényi, Extensions and modifications of the Kohonen SOM and applications in remote sensing image analysis, in: U. Seiffert, L. C. Jain (Eds.), Self-Organizing Maps: Recent Advances and Applications, Springer-Verlag, 2001, pp. 121–145.
11. J. Himberg, A SOM based cluster visualization and its application for false colouring, in: Proc. IEEE-INNS-ENNS International Joint Conf. on Neural Networks, Como, Italy, Vol. 3, 2000, pp. 587–592.
12. S. Kaski, T. Kohonen, J. Venna, Tips for SOM processing and colourcoding of maps, in: T. K. G. Deboeck (Ed.), Visual Explorations in Finance Using Self-Organizing Maps, London, 1998.
13. S. Kaski, J. Venna, T. Kohonen, Coloring that reveals cluster structures in multivariate data, in: Australian Journal of Intelligent Information Processing Systems, Vol. 6, 2000, pp. 82–88.
14. J. Vesanto, SOM-based data visualization methods, Intelligent Data Analysis 3 (2) (1999) 111–126.
15. K. Taşdemir, E. Merényi, Exploiting data topology in visualization and clustering of Self-Organizing Maps, Submitted to IEEE Transactions on Neural Networks.
16. K. Taşdemir, E. Merényi, Data topology visualization for the Self-Organizing Maps, in: Proc. 14th European Symposium on Artificial Neural Networks (ESANN'06), Bruges, Belgium, D-Facto, April 26-28, 2006, pp. 277–282.
17. T. Martinetz, K. Schulten, Topology representing networks, Neural Networks 7 (3) (1993) 507–522.
18. A. Ultsch, Clustering with som: U*c, in: Proc. 5th Workshop on Self-Organizing Maps (WSOM'05), Paris, France, September 5-8,, 2005, pp. 75–82.
19. S. W. Squyres, R. E. Arvidson, D. L. Blaney, B. C. Clark, L. Crumpler, W. H. Farrand, S. Gorevan, K. E. Herkenhoff, J. Hurowitz, A. Kusack, H. Y. McSween, D. W. Ming, R. V. Morris, S. W. Ruff, A. Wang, A. Yen, The rocks of the columbia hills, Journal of Geophys. Res.: Planets, 111, E02S11, 10.1029/2005JE002562.
20. W. H. Farrand, J. F. B. III, J. R. Johnson, S. W. Squyres, J. Soderblom, D. W. Ming, Spectral variability among rocks in visible and near infrared multispectral pancam data collected at gusev crater: Examinations using spectral mixture analysis and related techniques, Journal of Geophys. Res.: Planets, 111, E02S15, 10.1029/2005JE002495.
21. W. H. Farrand, J. F. B. III, J. R. Johnson, D. L. Blaney, Multispectral reflectance of rocks in the columbia hills examined by the mars exploration rover spirit: Cumberland ridge to home plate, Lunar and Planeary. Science XXXVIII (1957).
22. S. W. Ruff, P. R. Christensen, D. L. Blaney, W. H. Farrand, J. R. Johnson, J. E. Moersch, S. P. Wright, S. W. Squyres, The rocks of guser crater as viewed by the mini-tes instrument, Journal of Geophys. Res.: Planets, 111, E12S18, 10.1029/2006JE002747.
23. K. E. Herkenhoff, S. Squyres, R. Arvidson, the Athena Science Team, Overview of recent athena microscopic imager results, in: Lunar and Planetary Science XXXVIII, abstract 1421, 2007.